

INFLUENCE OF THE N_{α} -SPECTRUM ON LOWER HYBRID CURRENT DRIVE IN ASDEX

F. Leuterer, M. Brambilla, D. Eckhardt, K. McCormick, M. Münich, F. Söldner, M. Zouhar, G. Becker, H.S. Bosch, H. Brocken, A. Eberhagen, G. Fussmann, O. Gehre, J. Gernhardt, G. v.Gierke, E. Glock, O. Gruber, G. Haas, J. Hofmann, A. Izvozchikov¹, G. Janeschitz, F. Karger, M. Keilhacker², O. Klüber, M. Kornherr, K. Lackner, M. Lenoci³, G. Lisitano, F. Mast, H.M. Mayer, D. Meisel, V. Mertens, E.R. Müller², H. Murmann, H. Niedermeyer, A. Pietrzyk⁴, W. Poschenrieder, H. Rapp, H. Röhr, J. Roth, F. Rytter⁵, F. Schneider, C. Setzensack, G. Siller, P. Smeulders², K.-H. Steuer, F. Wagner, D. Zasche

Max-Planck-Institut für Plasmaphysik
EURATOM Association, D-8046 Garching

The lower hybrid current drive experiments in ASDEX so far have been performed mainly by operating successive waveguides of the grill at a relative phase of $\Delta\varphi = \pi/2$ and with equal amplitudes. The spectrum thus excited is considered in this paper as a reference spectrum and is shown as spectrum C 1 in Fig. 1. With such a spectrum it has been observed, like in many other related experiments, that the primary current rate of change, $-\dot{I}_{OH}$, necessary to maintain a constant plasma current I_p , decreased with increasing rf-power, P_{RF} . At a specific value of P_{RF} , depending on density and plasma current, \dot{I}_{OH} becomes zero and the plasma current is driven by rf alone, while at higher powers the transformer gets recharged /1/. The scaling of these effects was found to depend on the accessibility of the lower hybrid waves and to agree with theoretical predictions /2, 3/. It was also shown that the current density profile $j(r)$ for rf-current drive is different from that obtained for inductive current drive and is no longer directly determined by the electron temperature profile /4, 5/. In this paper we describe experiments with "tailored" spectra where phase and amplitude in each waveguide are specifically set to produce a N_{α} -spectrum with a definite wing at the high N_{α} -side. Such a wing is considered essential in explaining the magnitude of the driven currents as observed in the experiments /6/. These spectra are obtained by appropriately superimposing in the grill waveguides fields producing each by itself different N_{α} -spectra, resulting in

$$U_n = e^{i(n-1)\Delta\varphi_1} + a \cdot e^{i\alpha} e^{i(n-1)\Delta\varphi_2} \quad (1)$$

Here U_n is the wave amplitude in the n -th waveguide of the grill. One set of such spectra where we used $\Delta\varphi_1 = \pi/2$, $\Delta\varphi_2 = 5\pi/6$, and α and a were varied, is shown in Fig. 1. Other combinations of $\Delta\varphi_1$, $\Delta\varphi_2$, a , and α were used in order to tailor the wing of the spectrum in different ways (for example Fig. 6). In the experiment we have excited each one of these spectra with the same total input power of 400 kW. This was about a power limit for those experiments because of the very different powers (up to 130 kW) to be applied to the individual waveguides. A density of $n_e = 6 \times 10^{12} \text{ cm}^{-3}$ was then chosen in order to obtain a stationary current drive ($\dot{I}_{OH,RF} = 0$) in the case of the reference spectrum C 1.

¹Academy of Sciences, Leningrad, USSR; ²Assigned to JET Joint Undertaking, England; ³ENEA Frascati, Italy; ⁴University of Washington, Seattle, USA; ⁵CEN Grenoble, France

Figure 2 shows the primary current $I_{OH}(t)$ which is necessary to maintain a constant plasma current I_p before and during the application of LH-power with the spectra shown in Fig. 1. The curves are displaced for clarity. We recognise that for spectra with an increasing fraction of power at high N_{∞} the current drive becomes less efficient, i.e. $-I_{OH,RF}$ increases. The same $I_{OH,RF}$ would be obtained with a smaller amount of power, $P_{RF,Cn}^0$, if the applied spectrum were the reference spectrum C 1. In Fig. 3 we plot the ratio $P_{RF,Cn}^0/P_{RF,C1}$ where $P_{RF,C1}$ is the power resulting in $I_{OH,RF} = 0$ for the spectrum C 1. The LH-driven current scales, as:

$$\text{where } I_{RF} \sim \mu \cdot g \cdot P_{RF} / n_e,$$

$$\mu = \int_{N_{u2}}^{N_{u1}} P(N_n) dN_n / \int_{-\infty}^{\infty} P(N_n) dN_n, \quad g = (N_{u1}^2 / N_{u2}^2 - 1) / (N_{u1}^2 \ln N_{u1} / N_{u2})$$

and N_{u2} is determined by accessibility or the lower N_{∞} -boundary of the spectrum /7,8/. We therefore may write:

$$P_{RF,Cn}^0 / P_{RF,C1} = (\mu \cdot g)_{Cn} / (\mu \cdot g)_{C1}.$$

The factor $(\mu \cdot g)$ depends of course on the choice of the spectrum boundaries N_{u2} and N_{u1} . The two lines in Fig. 3 show the calculated ratio $(\mu \cdot g)_{Cn} / (\mu \cdot g)_{C1}$. For line a we chose $N_{u2} = N_{acc} = 1.5$ and the upper boundary N_{u1} was

determined by $r = \int_0^{N_{u1}} P(N_n) dN_n / \int_0^{\infty} P(N_n) dN_n = 0.97$. For line b N_{u2} was

either $N_{u2} = N_{acc} = 1.5$ or determined by $r = 0.1$ and N_{u1} was determined by $r = 0.9$, thus shifting N_{u2} to values greater than 1.5 for the spectra C 7 to C 13. We see that in the experiment the current drive efficiency is always greater than in the calculation b, while for calculation a this is true only for spectra C 3 and C 5, but less than calculated for C 9 to C 13. From this we conclude that in using the above equation for g , which is derived for a rectangular power spectrum /8/, we overemphasise the high N_{∞} -part of the spectrum while the low N_{∞} -part is more efficient with respect to current drive. To describe our experimental results in more detail we would thus need instead of the function g a function which does not only depend on the boundaries N_{u2} and N_{u1} of the spectrum but also upon its shape.

We further observed that the signal $\Delta + 1$ as deduced from the equilibrium field depends remarkably upon the applied spectrum. As an example we show in Fig. 4 the difference between $\Delta + 1 = \beta_{p,eq}^{\perp} + 1/2$ and β_p^{\perp} (from the diamagnetic loop). This difference changes when LH-power is applied due to the wave generated anisotropy in the electron velocity distribution, $\beta_{p,eq}^{\perp} - \beta_p^{\perp}$ which occurs on a fast time scale and is positive, and also because of a slowly decreasing l_1 . The dependence of l_1 as a function of the applied spectrum is shown in Fig. 5 for the set of spectra shown in Fig. 6. We see that $-\Delta l_1$ increases with increasing power in the high N_{∞} -part of the spectrum. This has also been observed in a phase scan where the shape of the spectrum remains roughly constant but the mean value $\langle N_{\infty} \rangle$ is shifted from 2 to 4 with a directivity dropping to zero. The change in l_1 is thus not only related to the amount of rf-driven current, but also to the shape of the spectrum, and the maximum Δl_1 does not coincide with a maximum current drive efficiency. This suggests that the higher N_{∞} -part of

the spectrum is absorbed further radially outward than the low N_{α} -part. The generated current density profile depends on the choice of the spectrum, and is not only determined by the direct rf-driven current, but also by an rf-modified conductivity profile due to bulk heating or suprathreshold electrons.

We should also note that while l_1 is decreasing additional power from the decreasing poloidal field energy is available in the plasma, leading to a further reduction in the loop voltage.

REFERENCES

- /1/ F. Leuterer et al., Phys.Rev.Lett. 55 (1985) 75
- /2/ F. Leuterer et al., Plasma Phys. and Contr. Fus. 27 (1985) 1399
- /3/ F. Leuterer et al., Proc. 12th Europ. Conf. on Contr. Fusion and Plasma Physics, Budapest 1985, Vol. II, p. 240
- /4/ K. McCormick, *ibid.*, Vol. I, p. 199; also this conference
- /5/ F. Söldner et al., this conference
- /6/ S. Succi et al., Proc. 10th IAEA-Conf. Plasma Physics and Contr. Nucl. Fusion, London 1984, Vol. I, p. 549
- /7/ G. Tonon, D. Moulin, 4th Int.Symp. Heating in Toroidal Plasma, Rome 1984, Vol. II, (1984) 1343
- /8/ C.F. Karney, N. Fisch, Phys.Fluids 22 (1979) 1817

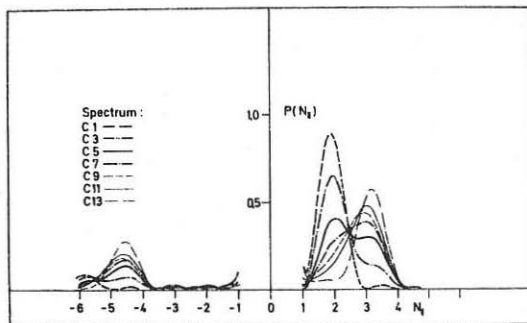


Fig. 1

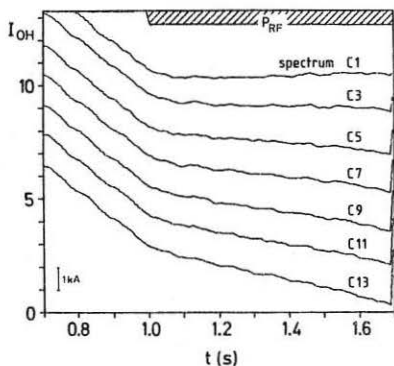


Fig. 2

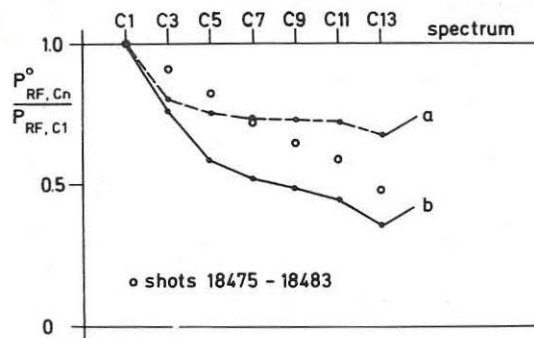


Fig. 3

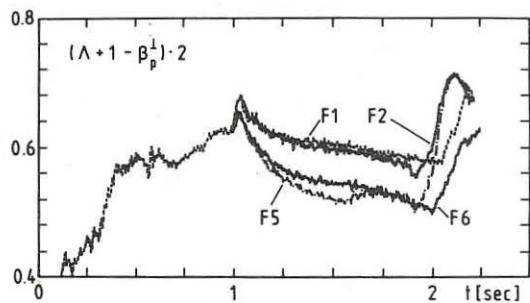


Fig. 4

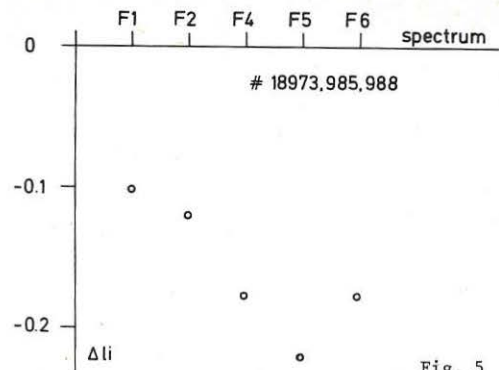


Fig. 5

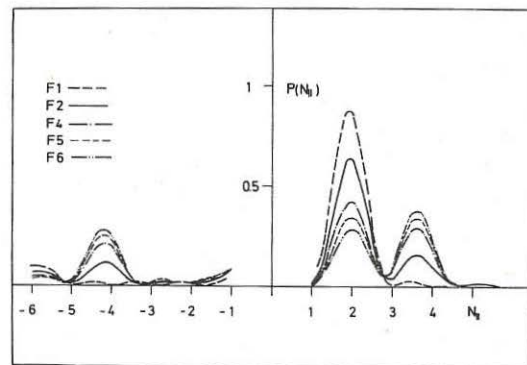


Fig. 6